Crystallization and welding variations in a widespread ignimbrite sheet; the Rattlesnake Tuff, eastern Oregon, USA

Streck, Martin; Grunder, Anita L.

ORIGINAL PAPER

M. J. Streck · A. L. Grunder

Crystallization and welding variations in a widespread ignimbrite sheet; the Rattlesnake Tuff, eastern Oregon, USA

Abstract The 7.05 Ma Rattlesnake Tuff covers ca. 9000 km², but the reconstructed original coverage was between 30000 and 40000 km². Thicknesses are remarkably uniform, ranging between 15 and 30 m for the most complete sections. Only 13% of the area is covered with tuff thicker than 30 m, to a maximum of 70 m. The present day estimated tuff volume is 130 km³ and the reconstructed magma volume of the outflow is 280 km³ DRE (dense rock equivalent). The source area of the tuff is inferred to be in the western Harney Basin, near the center of the tuff distribution, based mainly on a radial exponential decrease in average pumice size, and is consistent with a general radial decrease in welding and degree of post-emplacement crystallization. Rheomorphic tuff is found to a radius of 40–60 km from the inferred source.

Four facies of welding and four of post-emplacement crystallization are distinguishable. They are: non-welded, incipiently welded, partially welded and densely welded zones; and vapor phase, pervasively devitrified, spherulite and lithophysae zones. The vapor phase, pervasively devitrified and lithophysae zones are divided into macroscopically distinguishable subzones. At constant thickness (20 ± 3 m), and over a distance of 1–3 km, nonrheomorphic sections can vary between two extremes: (a) entirely vitric sections grading from nonwelded to incipiently welded; and (b) highly zoned sections. Highly zoned sections have a basal non- to densely welded vitric tuff overlain by a spherulite zone that grades upward through a lithophysae-dominated zone to a zone of pervasive devitrification, which, in turn, is overlain by a zone of vapor-phase crystallization and is capped by partially welded vitric tuff. A three-dimensional welding and crystallization model has been developed based on integrating local and regional variations of 85 measured sections.

Strong local variations are interpreted to be the result of threshold-governed welding and crystallization controlled by residence time above a critical temperature, which is achieved through differences in thickness and accumulation rate.

Key words Pumice · Welding · Devitrification · Lithophysae · Tridymite · Rheomorphism · Rattlesnake Tuff · Ignimbrite

Martin J. Streck
GEOMAR, Abt. Vulkanologie & Petrologie,
Wischhofstrasse 1–3, D-24148 Kiel, Germany,
Tel.: (49) 431-7202211. Fax: (49) 431-7202217
E-Mail: mstreck@geomar.de

Anita L. Grunder (✉)
Department of Geosciences, Oregon State University,
Corvallis, OR 97331-5506, USA
Tel.: (503) 737-1201. Fax: (503) 737-1200.
E-mail: grundera@bcc.orst.edu

Introduction

Zones and zonal variations in ignimbrites are based mainly on the classic works of Smith (1960, 1980) and Ross and Smith (1980). Descriptions of lateral variations in welding and post-emplacement crystallization for single extensive ignimbrite sheets were rare 30 years ago (Smith 1980: 149) and few have been added since. This study focuses on the lateral and vertical variations of welding and crystallization in the Rattlesnake Tuff, a uniformly thin, widespread ignimbrite sheet in eastern Oregon, formerly referred to as the Rattlesnake Ash-Flow Tuff (Walker 1979). The tuff is well exposed over several tens of thousands of square kilometers and welding, crystallization and rheomorphic processes are responsible for a large number of facies with excellent preservation. The tuff includes features characteristic of non-welded to lava-like ignimbrites (e.g. Branney and Kokelaar 1992). A facies model based on the Rattlesnake Tuff highlights the complexities that might be expected in voluminous, thin and widespread ignimbrites (i.e. Mansfield and Ross 1935; Stearns and Isotoff 1959;

Fig. 1 Regional setting and outcrop pattern of the Rattlesnake Tuff. Light stipple represents Blue Mountains Province, dense stipple shows Rattlesnake Tuff; proposed source area indicated by closed circle. Dotted lines with numbers are simplified isochrons in million of years for north-west migrating silicic volcanism, after MacLeod et al. (1976). Solid lines indicate faults and stars indicate Cascade composite volcanoes
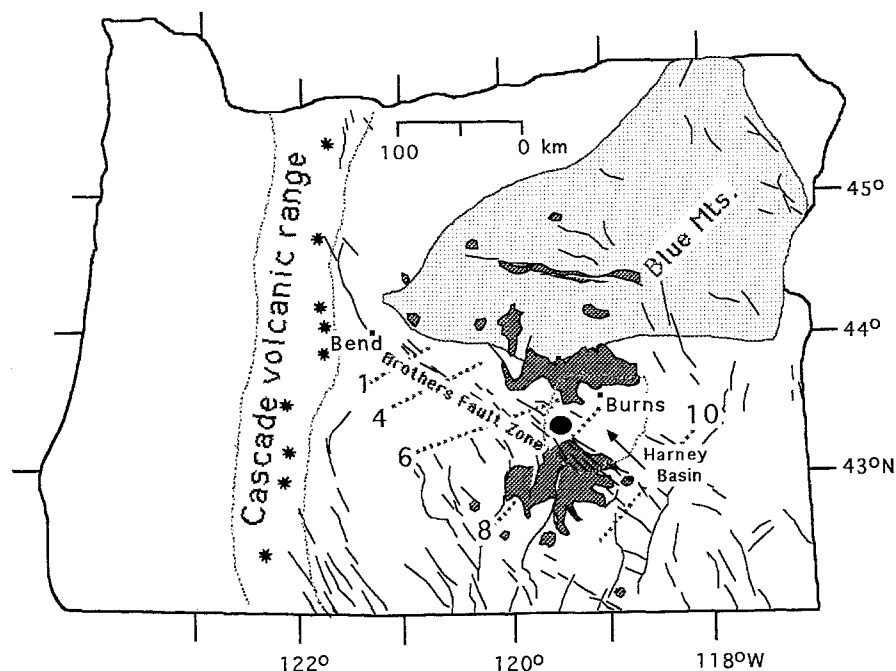
Walker 1970, 1979; Greene 1973; Bonnichsen and Citron 1982; Ekren et al. 1984). The broader importance of zones and zonal variations in ignimbrites is the constraint they place on the eruption and emplacement dynamics of large-scale volcanic processes, the products of which are common in the geological record, but which have never been witnessed.

Setting, age and general aspect

The Rattlesnake Tuff is an important regional stratigraphic and structural marker. It is exposed over at least 9000 km^2 in eastern Oregon from the Blue Mountains Province to the north into the northern Basin and Range Province to the south (Fig. 1). The High Lava Plains separate the two provinces and coincide broadly with the Brothers Fault Zone (Lawrence 1976). Although characterized by high-alumina olivine tholeiite lavas, the High Lava Plains include tuffaceous sediments and silicic volcanic rocks in dome complexes and ignimbrites (Walker 1970, 1974; MacLeod et al. 1976; Walker 1979; Hart et al. 1984; Carlson and Hart 1987; Draper, 1991). The ages of silicic volcanic rocks generally decrease from about 10 Ma near the south-eastern end of the Brothers Fault Zone to less than 1 Ma at the north-western end (MacLeod et al. 1976). The Rattlesnake Tuff is part of this age progression. The weighted average of 15 single-crystal ^{40}Ar–^{39}Ar analyses of alkali feldspar yielded an age of 7.05±0.01 Ma (Table 1), consistent with the oldest previously reported K–Ar dates, which range from 5.95±0.18 to 6.7±0.4 Ma (Walker 1979).

The Rattlesnake Tuff is a single cooling unit that includes the Double-O Ranch Tuff, the Twelvemile Tuff of Greene et al. (1972) and the Rattlesnake Tuff

(Thayer 1952; Enlows 1976), based on mapping and correlation of trace element analyses performed by instrumental neutron activation (Beeson 1969; Davenport 1971; Walker 1979; and this study). It typically occurs as 10–20 m thick plateau-capping rimrock. Evidence for as many as three flow units was found at one location ~100 km north-northwest of Burns (near Dayville). There, sharp interfaces between nonwelded zones, each 1–2 m thick, separate flow units. The top of the section is made of surge deposits, which probably originated through secondary ash flows. The existence of at least two flow units elsewhere is based on a reversal in the proportions of various glass shard populations. A sharp interface between the vitric tuff and the overlying crystallized tuff, south-west of Harney Lake, was mistakenly interpreted as a break between flow units by Parker (1974).

The Rattlesnake Tuff is nonwelded to densely welded with spherulite, lithophysae, pervasively devitrified and vapor phase crystallization zones. The phenocryst content is around 1% or less for the bulk tuff. Where pumiceous, the tuff commonly has distinctive white, gray, black and banded pumice clasts set in a salt and pepper matrix of white and gray glass shards (Fig. 2). White and gray pumices and shards are high-silica rhyolite (75–77.5 wt.% SiO$_2$) and black pumices are slightly alkalic dacite (62–70 wt.% SiO$_2$); there are no dacite shards.

Fallout deposits are locally preserved at the base of the Rattlesnake Tuff (Fig. 2c), near Burns and Harney Lake. They are interpreted to be related to the ash-flow tuff based on chemical similarity to the most evolved pumice clasts in the ash-flow tuff and the absence of soil development. The greatest thickness of the fallout is about 1 m. In most places where the base of the tuff is exposed, there is no fallout deposit.

Table 1 ^{40}Ar–^{39}Ar analytical data for the Rattlesnake Tuff anorthoclose/sodic sanidine

Laboratory ID No.	Ca/K	^{36}Ar/^{39}Ar	^{40}Ar*/^{39}Ar	% ^{40}Ar*	Age (Ma) $\pm 1\sigma$
Sample: HP91-12					
5357-01	0.302	0.00014	0.778	93.8	6.99 ± 0.02
5356-06	0.096	0.00013	0.783	93.2	7.03 ± 0.02
5357-03	0.098	0.00031	0.783	87.8	7.03 ± 0.02
5357-04	0.082	0.00010	0.784	94.2	7.04 ± 0.02
5357-07	0.110	0.00012	0.784	93.5	7.04 ± 0.02
5356-07	0.085	0.00014	0.784	92.9	7.04 ± 0.02
5356-08	0.063	0.00011	0.784	93.9	7.04 ± 0.02
5356-01	0.062	0.00010	0.785	94.0	7.04 ± 0.02
5357-02	0.105	0.00007	0.785	95.2	7.04 ± 0.02
5356-04	0.082	0.00011	0.786	93.9	7.05 ± 0.02
5356-05	0.111	0.00031	0.786	87.8	7.05 ± 0.02
5356-03	0.025	0.00005	0.786	95.6	7.06 ± 0.02
5357-05	0.099	0.00013	0.787	93.4	7.06 ± 0.02
5357-06	0.076	0.00010	0.787	94.2	7.07 ± 0.02
5356-02	0.036	0.00008	0.787	94.5	7.07 ± 0.02
Wtd. Ave.					7.05 ± 0.01

Age determinations were performed by Alan Deino at the Geochronology Center of the Institute of Human Origins, Berkeley, California, USA. Notes: Errors in age quoted for individual runs are 1σ analytical uncertainty. Weighted averages are calculated using the inverse variance as the weighting factor (Taylor 1982), whereas errors in the weighted averages are the 1σ standard error of the mean and incorporate error in J (see below) (Sampson and Alexander 1987). Ca/K is calculated from ^{37}Ar/^{39}Ar using a multiplier of 1.96. ^{40}Ar* refers to radiogenic argon. $\lambda = 5.543 \times 10^{-10}$ y^{-1}. $J = 0.004986 \pm 0.00001$ Isotopic interference corrections: $(^{36}$Ar/^{37}Ar$)_{Ca} = 2.58 \times 10^{-4} \pm 6 \times 10^{-6}$, $(^{39}$Ar/^{37}Ar$)_{Ca} = 6.7 \times 10^{-4} \pm 3 \times 10^{-5}$ $(^{40}$Ar/^{39}Ar$)_K = 2.19 \times 10^{-2} \pm 2 \times 10^{-4}$

Distribution, thickness and volume

Today's outcrops

Thickness information from 240 measured sections was compiled for the whole tuff sheet (Fig. 3). The Rattlesnake Tuff is semicontinuously exposed over an area of ca. 9250 km^2 (Table 2, Fig. 3). The area covered by tuff thicker than 30 m is 1250 km^2 and describes a southern and a northern arc distributed around the inferred source area (discussed in the following). The rest (87%) of the total area is covered by tuff with a thickness of less than 30 m. Most of the tuff is remarkably uniform in thickness, between 5 and 30 m, despite a radius of distribution greater than 100 km. Individual sections as thick as 30 m were mainly established by cliff measurements with rope; thicker sections were determined either by hand-leveling or were estimated from contours on a 7.5 minute topographic map. Most thickness determinations are minima, mainly because of erosion effects. Based on lithology and crystallization facies, however, no more than a few meters are missing in most places. Throughout the distribution area, the lower boundary of the tuff crops out at numerous localities (Figs. 2c and 6). Where the base was not exposed, it could be constrained by comparison of the thicknesses of zonal variations in similar, but more complete sections. Constraints on the original upper boundary are more ambiguous. Upper nonwelded tuff is preserved in only one locality. However, highly zoned sections (Fig. 2c) commonly include upper partially welded, vitric tuff, suggesting that only 1–3 m of the top were eroded.

This estimate assumes that the original upper non- to partially welded, vitric tuff was comparable in thickness with the basal vitric zone (cf. Riehle 1973). Even if the upper vitric sections were twice as thick as the basal sections, the thickness estimates would not be strongly affected. Exposure thicknesses of less than 10 m in strongly welded or crystallized tuff (see regional facies variations) within a radius of 80 km from the inferred source are probably due to erosion and do not represent nearly complete sections.

Original areal coverage

Reconstruction of the area originally covered with tuff is critical for estimates of the volume erupted. The reconstructed area, originally covered by tuff but later eroded or buried by younger deposits, was divided into four qualitative categories, 'certain', 'very likely', 'likely' and 'probable', indicating increasing degrees of uncertainty in the estimate (Fig. 3, Table 2). 'Certainly' includes proximal areas around the vent and those places surrounded by today's outcrops (Streck 1994). 'Very likely' includes less proximal areas and areas fairly well surrounded by present outcrops. 'Likely' was assigned to lobes needed to connect well correlated, but distal, remnants of the tuff, or areas not surrounded by outcrops. The solid line in the inset of Fig. 3 encloses the cumulative area of the categories 'certain', 'very likely' and 'likely'. The category 'probable' includes areas that make for a more equant distribution of the Rattlesnake Tuff and the limit is indicated by the bro-
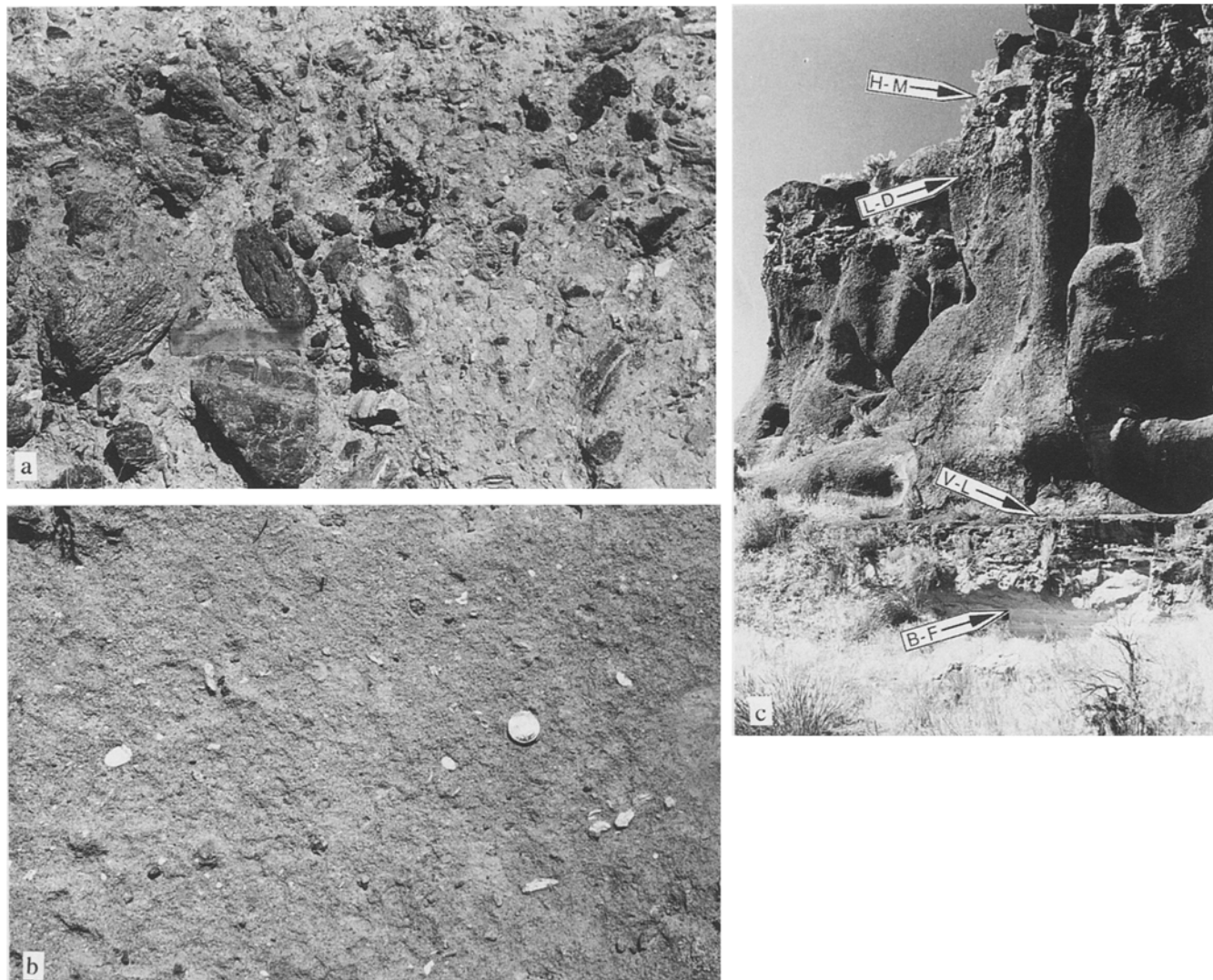
Fig. 2 a Pumice-rich tuff with 30–50% pumice, 37 km from inferred vent. Outcrop yielded an average of five largest pumices of 57.4 cm. Plastic ruler is 12 cm long. **b** Pumice-poor (ash-rich) section, 148 km from inferred vent, containing ca. 2% pumice lapilli. Average maximum lapilli size for this locality is 3.7 cm. Coin for scale is 1.9 cm. **c** Section of Rattlesnake Tuff, 16 m thick. **B–F** Boundary between laminated basal fallout and nonwelded, vitric tuff; **V–L** transition between densely welded vitric tuff and overlying lithophysal zone – lower vitric tuff grades from nonwelded at the **B–F** boundary to densely welded at the **V–L** transition; **L–D** transition between lithophysal zone and overlying hackly jointed, pervasively devitrified zone; and **H–M** transition within the pervasively devitrified zone between lower hackly jointed and upper massive part

ken line in the inset of Fig. 3. The Rattlesnake Tuff probably covered 35 000 km² (Table 2), which might still be a minimum value.

The aspect ratio of ash-flow tuffs (average tuff thickness/diameter of circle enclosing all outcrops) has been used as an indicator of energy of the ash flow (Walker 1983). By this standard, the aspect ratio of the Rattlesnake Tuff is 2.5×10^{-4} to 5×10^{-5}, using conservative to optimistic values of 50 m/200 km and 15 m/300 km,

respectively. Both aspect ratios fall within the range of areally extensive, high-energy ash-flow tuffs (c.f. Fig. 1 of Walker 1983).

The wide distribution and little variation in deposit thickness (typically 15–30 m, regardless of degree of welding) were probably facilitated by low topographic relief at the time of eruption. The base of the Rattlesnake Tuff has a maximum of 1000 m of topographic relief; it is highest 50 km north of the inferred vent and lowest in the central John Day Valley (Fig. 3). The present relief is mainly post-depositional, as indicated by the fact that all high-altitude outcrops are well above the present valley floors and typically have a high degree of welding and crystallization. A more rugged topography would have generated thicker valley-filling deposits thinning outward to a more patchy distribution, as described for the Campanian ignimbrite (Fisher et al. 1993). Over most of its extent, the Rattlesnake Tuff has only a few meters of relief over kilometers of outcrop and has a landscape-mantling appearance. Paleotopography controlled thickening of the tuff is possibly indicated by the distribution of tuff thicker
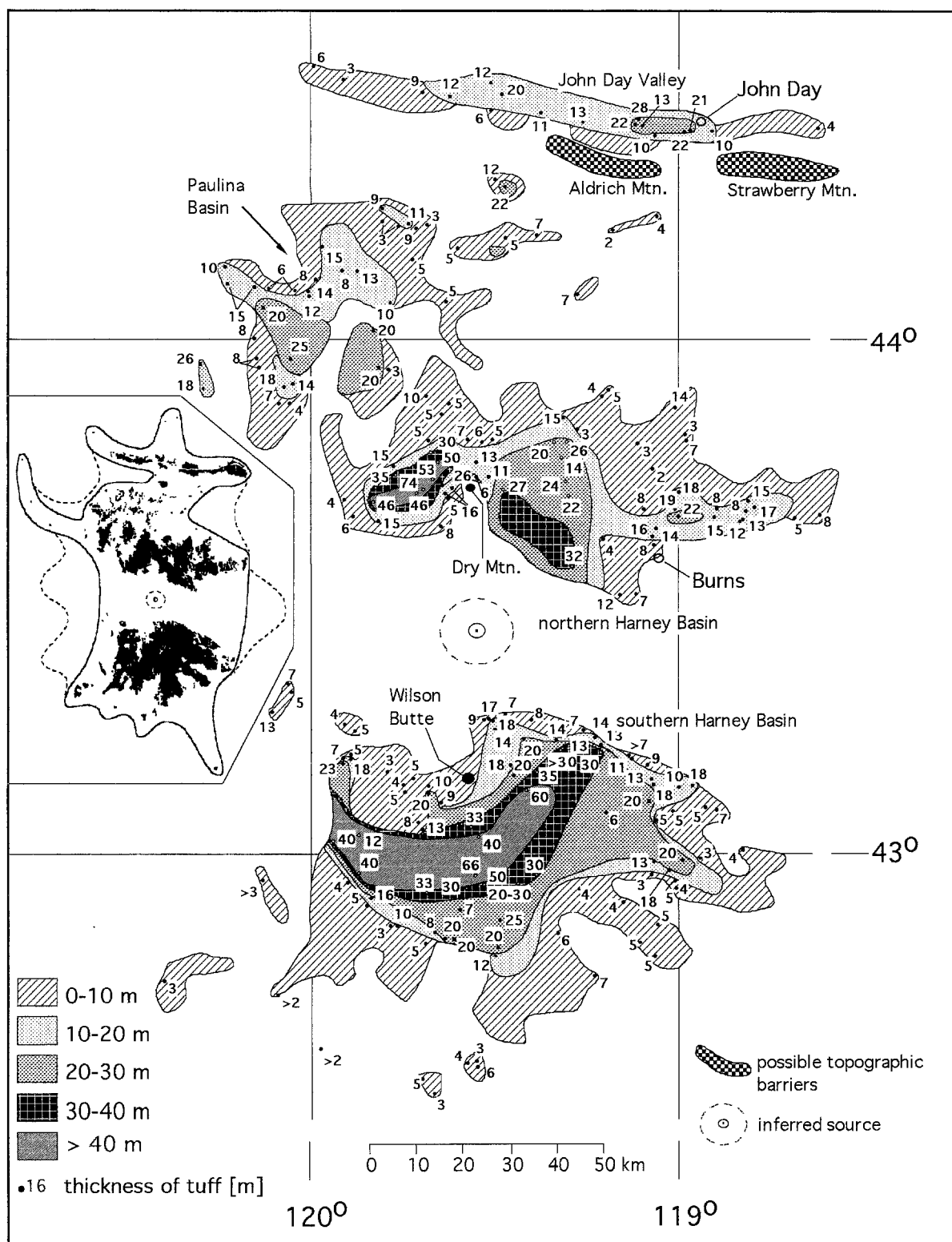
155

Fig. 3 Isopach map. Thickness of the Rattlesnake Tuff is shown in meters. Dashed circle is inferred source area. Most distal tuff remnants not shown. Insert shows outcrop map with reconstructed original extent. Solid lines encloses the cumulative area of the categories 'certain', 'very likely' and 'likely'; the broken lines indicate the category 'probable'; see text for explanation of reconstruction categories. Sources for outcrops are: Brown and Thayer (1966), Davenport (1971), Greene et al. (1972), Johnson (1960), Swanson (1969), Smith et al., 1984, Walker (1963), Walker and Repenning (1965), Walker et al. (1967), Wallace and Calkins (1956) and Wilcox and Fisher (1966). Outcrop pattern in John Day Valley shows Rattlesnake Tuff and closely related conglomeratic units of Brown and Thayer (1966)

Table 2 Area and volume estimates

	Area (km^2)			Volume (km^3)				
	Area	Cumulative area	T_h^*	Tuff		ρ^t/ρ^{gl+}	Magma erupted$^{\neq}$	
				Volume	Cumulative volume		Volume	Cumulative volume
Isopach area								
5–10 m	4845	4845	5	24.2	24.2	0.77	18.6	18.6
10–20 m	1535	6380	15	23.0	47.2	0.86	19.8	38.4
20–30 m	1624	8004	25	40.6	87.8	0.94	18.2	56.6
30–40 m	591	8595	30	17.7	105.5	1	17.7	74.3
>40 m	653	9248	40	26.1	131.6	1	26.1	100.4
Sub-total	9248			131.6			100.4	
Reconstructed								
Certain	3322	3322	10–15	46.3	46.3	0.9	41.7	41.7
Very likely	5042	8364	8–12	52.1	98.4	0.9	46.9	88.6
Likely	7683	16047	5–10	51.1	149.5	0.9	46	134.6
Probable	9701	25748	5– 8	50.8	200.3	0.9	45.7	180.3
Total	34996			331.9			280.7	

* Conservative thicknesses (m) used for volume calculations.
$^+\rho^t/\rho^{gl}$ = Density of tuff/density of dense rock (ρ=2.34).

$^{\neq}$Erupted magma calculated as dense rock equivalent with ρ^t/ρ^{gl} ratio.

than 40 m. The two areas (Fig. 3) are located on the lee side of older volcanic edifices (Dry Mountain and Wilson Butte). Other likely topographic barriers causing either very thin or no deposits were the Strawberry and Aldrich Mountains (Fig. 3) and local areas around older domes or composite volcanoes.

Volume

Previous volume estimates of the Rattlesnake Tuff spanned a wide range from 10 km^3 (Draper 1991) to 150–200 km^3 (Walker 1970) to 1500 km^3 (Parker 1974). We estimate the total magma volume in outflow as 280 km^3 (Table 2). No fallout tuff or possible intra-caldera ignimbrite is considered, making this a minimum estimate for the eruption. Using the established isopach map with conservative average thicknesses, the volume preserved in the present day outcrops is 132 km^3 (Table 2). The tuff volume for the reconstructed area was calculated using conservative thicknesses comparable with nearby sections. The total volume (present day + reconstructed) is 332 km^3 (Table 2). Because much of the tuff is not densely welded, the magmatic volume is less. Dense glassy rock from the Rattlesnake Tuff has a specific gravity of 2.34 g/cm^3. A range of specific gravities, based on measurements of representative samples, was used for the different isopach areas to approximately account for welding variations.

Depositional facies

Pumice clasts

Pumice clast investigations were undertaken at non-welded to incipiently welded sections where pumices are not deformed by welding (Fig. 2a and 2b). The largest pumices at any given outcrop are always of the white and gray type. At one extreme, outcrops will be composed of subequal proportions of white, gray and mingled (banded) pumices. Some outcrops, usually beyond 80 km from the inferred source, consist almost exclusively of white pumice clasts and shards. In general, the proportion of white pumice and shards is greatest at the base and in distal outcrops. Typically, but not exclusively, the abundances of gray and black pumices and of gray shards increase upward within the first 1 to 2 m. These vertical and lateral variations can be interpreted as the tapping of successively deeper levels of a zoned magma chamber (Smith 1979) as a first order process, complicated by deposition and erosion mechanics of overlapping ash flows.

The results from calculating the average sizes of the five largest pumice clasts at many localities show a decrease in the average maximum size away from the inferred source (Figs. 4a and 5a). Pumice clast averages range from 57 to 1–3 cm. The rate of decrease follows an exponential curve rather than a linear curve (Fig. 5a). No vertical grading of pumices was observed, except for the lack of the largest pumices within 1 m of the base of the tuff. A decrease of average pumice size with distance has been found in some pyroclastic flow deposits (Kuno et al. 1964; Fisher 1966; Yokoyama 1974; Wright and Walker 1977). However, in many tuffs there is no simple relationship of average pumice size with distance; in some instances, size and distance correlate positively (Cas and Wright 1987: 194).

Along with the decrease in the average maximum pumice size with distance from the source, there is a decrease in the abundance of pumices from ca. 30 to 50% in proximal localities to 2% distally (Fig. 2a and 2b). Thus, the Rattlesnake Tuff changes its character laterally from being a pumice-rich tuff to an ash-rich tuff.
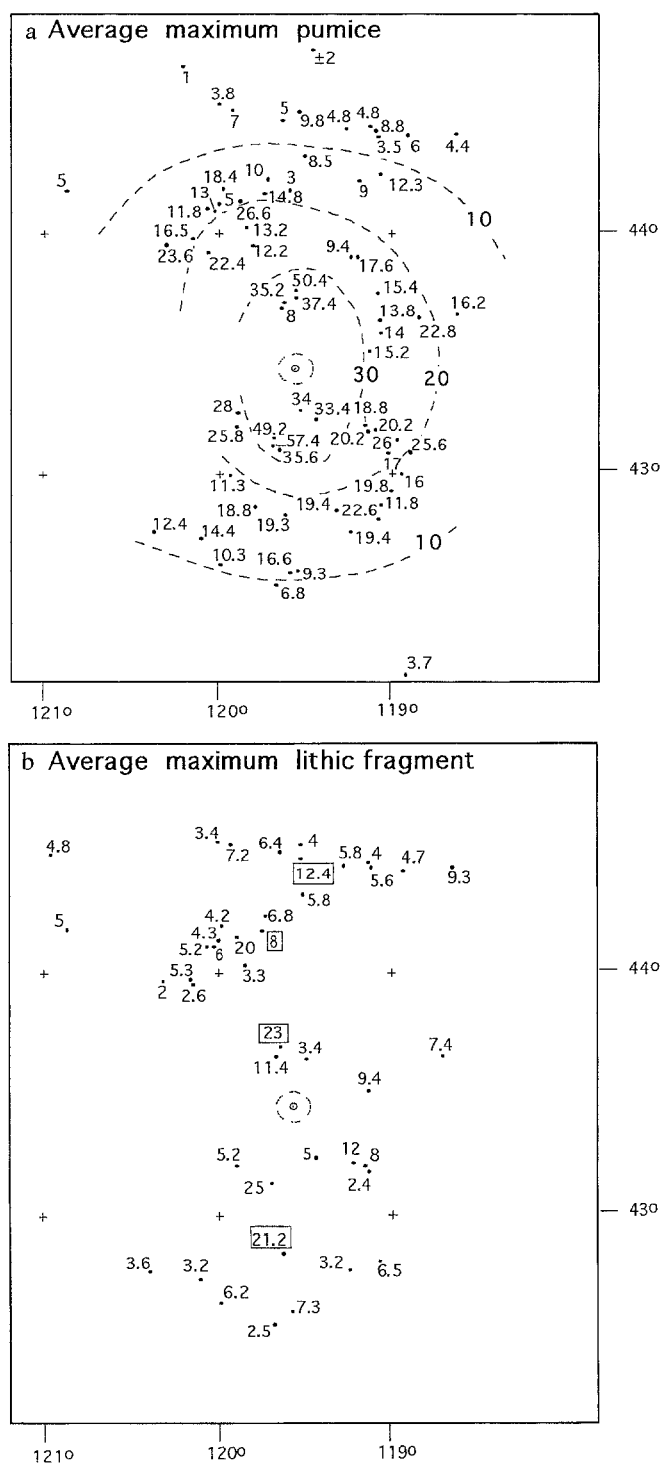
Fig. 4 a Average maximum pumice size. Values are in centimeters calculated from the five largest pumice clasts and are contoured approximately. Dashed circle is the inferred source. b Average maximum lithic fragment size in centimeters. Refer to Fig. 5b for the number of averaged lithic fragments for each site. Framed numbers indicate sites with a lithic-enriched zone near the base of the tuff; see text for details
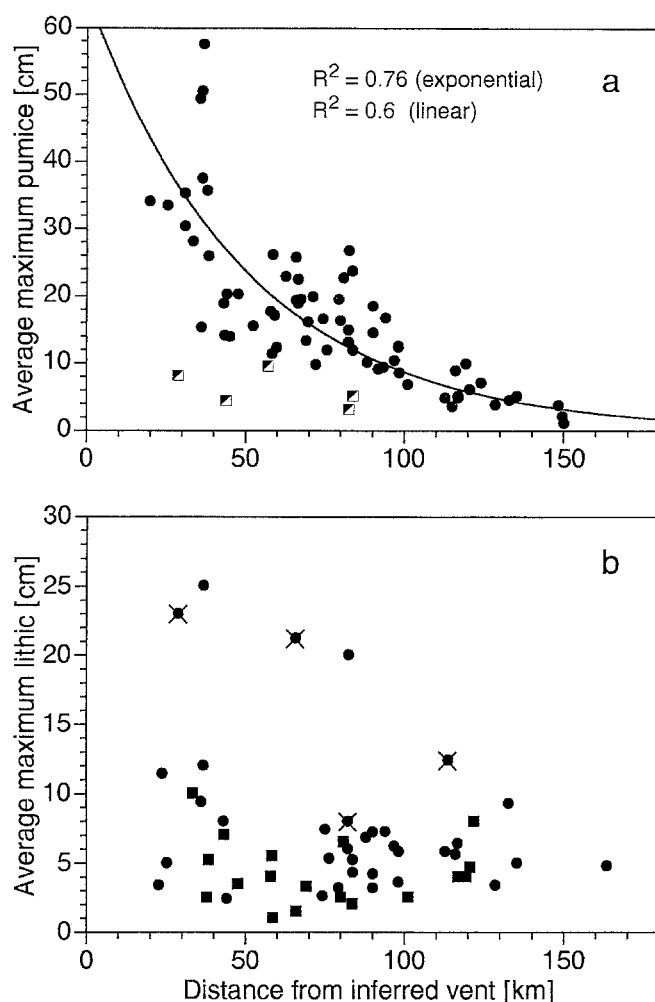

Fig. 5 a Distance versus average maximum pumice size. R^2 values compare an exponential with a linear regression fit. Solid line indicates exponential fit through data points; values with half-filled squares, representing poor outcrops, were omitted for regression calculation. b Distance versus average maximum lithic fragments. Circles represent sites with averages calculated from four or five lithic fragments; squares are sites where three or less lithic fragments were found and averaged; circles with crosses are sites with basal lithic-enriched zone

Lithic fragments

Accidental lithic fragments make up 1% or less of the tuff. Lithic fragment assemblages are dominated by basalt and basaltic andesite and may be monolithological. Wherever other lithologies were exposed at the time of passage of the ash flows, lithic fragment assemblages in the tuff are more diverse, as seen in the eastern Paulina Basin (Fig. 3). At several localities, pronounced lithic-enriched zones occur within the basal 1 m of the tuff. A local derivation of lithic clasts for these zones is indicated by the similarity of the clasts to those in the substrate and by ramp-like alignments of lithic fragments from the substrate into the tuff at an angle of ca. 20° (Fig. 6). In the John Day Basin, such a lithic-enriched zone has rounded lithic fragments that

Fig. 6 Ramp-like lithic fragment zone. Alignment of lithic fragments from the substrate into the tuff is thought to represent a picking-up feature at a site 66 km from inferred source. Note hammer among largest lithic fragments near the base of the ignimbrite

match the substrate conglomerate lithologies. There, evidence for the possible involvement of water includes the presence of degassing pipes nearby (Enlows 1976), the occurrence of secondary ash flow deposits and stronger columnar jointing.

Because the tuff normally contains very few lithic fragments, grading characteristics are difficult to evaluate. The average maximum lithic size is rarely greater than 15 cm and the greatest average maximum lithic size crudely decreases with distance from the inferred source (Figs. 4b and 5b), excluding places where the local entrainment of large clasts was an obvious problem.

Speculations on pumice and lithic vatiations

In ignimbrites, the average lithic fragment size typically correlates better with distance than the average pumice size (Sparks 1975; Cas and Wright 1987: 183; Suzuki-Kamata and Kamata 1990) because lithic fragments are significantly denser than the ash flow, whereas pumices may be more or less dense than the flow. The controlling factors in introducing distance dependencies are: (a) size and density of clast; and (b) density, viscosity and possibly yield strength and turbulent velocity of the ash flow (Cas and Wright 1987: 193).

In the Rattlesnake Tuff, the size–distance correlation is fairly strong for pumices, but not for lithic fragments. This apparent paradox could be explained with a model where material separates out of the overriding highly expanded pyroclastic flows to produce denser, non-expanded near-surface ash-flows which either do not travel far enough or are not sufficiently dense to cause reverse grading of the pumice clasts. For the

Campanian ignimbrite, Fisher et al. (1993) proposed a similar model in which the transport medium consisted of extremely expanded ash flows to travel over several hundred meter high ridges and the deposition medium consisted of near-surface, locally developed, much less expanded ash flows. The exponential decrease in average pumice clast diameter away from the source is analogous to the exponential pumice size decrease commonly observed in fallout tephra (e.g. Lirer et al. 1973; Bloomfield et al. 1977; Booth et al. 1978; Walker 1980), also indicating that a highly expanded 'transport medium' existed which exerted the principal control on the pumice distribution in the Rattlesnake Tuff.

The poor correlation of lithic fragments with distance can be interpreted to mean that at no point were the ash flows capable of transporting large lithic fragments over long distances, consistent with the pumice transport model. The greatest variations in lithic size distribution, however, are expected within 15 km of the source (cf. Wright and Walker; 1977; Suzuki-Kamata and Kamata 1990) and the proximal 20 km of the Rattlesnake Tuff are covered with basalt. The interpretation of lithic fragment distribution is further complicated by the local entrainment of clasts from the ground, consistent with increased turbulence around topographic obstacles (cf. Buesch 1992) or around areas where interaction with water can be inferred.

Regardless of the method of entrainment, the decrease in the size of the largest average lithic clasts carried by the tuff with distance (upper envelope of data, Fig. 5b) suggests that the carrying capacity of the flow decreased with distance.

Source area

No caldera structure related to the Rattlesnake Tuff is exposed. By analogy with pyroclastic deposits of similar volume, we might expect a caldera with an approximate diameter of 20 km (cf. Smith 1979; Spera and Crisp 1981). Several source areas, all lying within the Harney Basin, have been proposed (Fig. 7). Walker (1969) and Parker (1974) proposed the Buzzard Creek area, based on rheomorphic features interpreted as venting features. Walker (1970, 1979) proposed a caldera under Harney Lake. MacLeod et al. (1976) favored a site in the western Harney Basin based on the clustering of silicic domes of similar age.

To evaluate the potential source area of the Rattlesnake Tuff, we used an internally consistent model of increasing pumice size toward the vent and compared the proposed source with the areal distribution, distribution of facies and flow direction indicators in the tuff. The pumice data locations were cast in terms of a polar coordinate system with the origin as the presumed source. By relocating the origin of this coordinate system for different proposed venting areas with recalculation of the polar coordinates to the same pumice data set, we can evaluate how well the average pumice size
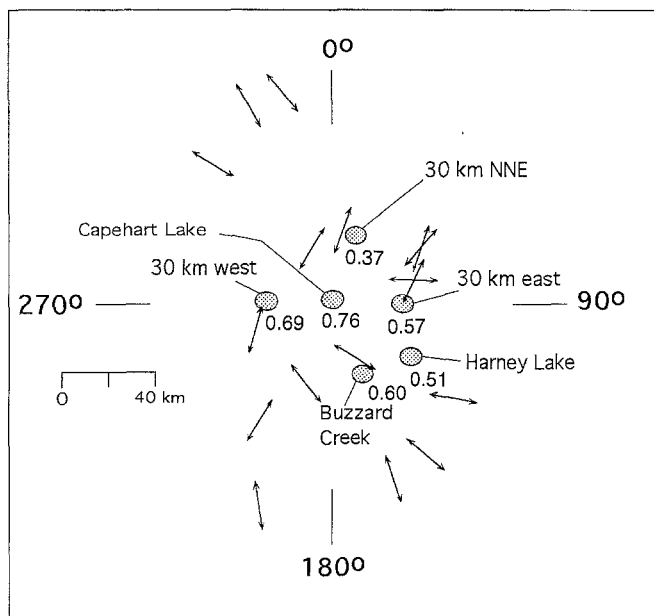
Fig. 7 Average alignments of long axes of pumices; arrows indicate directions of average alignments. Source area locations which were evaluated as potential venting sites are shown with stippled ovals; numbers next to the stippled ovals are exponential fit to recalculated pumice data to different source areas (point source); see text. Linear regression fit gave a poorer correlation for each site. Capehart Lake site is the proposed venting site shown in other figures
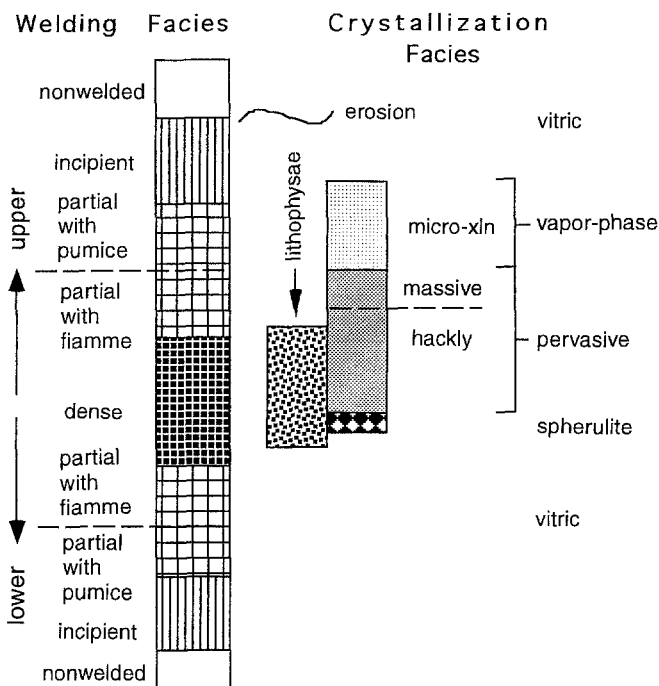

Fig. 8 Schematic vertical distribution of welding and crystallization for a complete, highly zoned section; all welding and crystallization facies occur in highly zoned sections, except the crypto-crystalline vapor phase zone which is not shown. For a more complex and realistic representation of the variability in zonation, see Fig. 15

and distance correlate for different source areas. Exponential regression lines were calculated to see which source area would give the best fit to the available data (Fig. 7). The best fit is for the source area 'Capehart Lake' located in the western Harney Basin (18 km SSW of the to town of Riley) (Fig. 7). This finding is compatible with the measured average alignments of the long axes of pumices (Fig. 7). The Capehart Lake source area also lies in the middle of the distribution of strongest crystallization and rheomorphic features of the Rattlesnake Tuff (Fig. 14) and within the arcs of thickest tuff (Fig. 3). Moreover, the proposed vent is near the center of the tuff's areal distribution (Fig. 3). It is almost identical with the source area proposed by Mac-Leod et al. (1976), based on the regional age distribution pattern of volcanism (Fig. 1).

Welding and crystallization facies

Most of the welding and crystallization terminology used here is after Ross and Smith (1980) and Smith (1960, 1980) with some additions from Iddings (1885–1886).

Welding facies

Five welding degrees are distinguished: nonwelded, incipiently welded, partially welded with pumice, partial-

ly welded with fiamme and densely welded. Transitions between welding degrees are highly gradational. The tuff may be highly zoned, exhibiting all of the welding facies, or it may be nearly unzoned, exhibiting only nonwelded and incipiently welded facies. Highly zoned sections grade from nonwelded at the base and top (now eroded) inward through incipiently welded to partially welded to a densely welded core (Fig. 8). From nonwelded to densely welded, the tuff loses pore space, as reflected by an increase in density from < 1.5 to 2.34 g cm^{-3}, the color changes from white or light gray to black, the luster changes from dull to vitreous (where not obscured by postemplacement crystallization) and pumice clasts and shards change from undeformed to entirely collapsed with complete coalescence of glassy material (Table 3).

Nonwelded tuff is characterized by lack of deformation of pumice clasts and shards and by little to no adhesion between clasts. Nonwelded tuff is preserved only in some basal sections, where it ranges in thickness from 0.5 to 4–6 m in proximal to distal sections, respectively.

Incipiently welded tuff exhibits no deformation of pumices or glass shards and, although some adhesion occurs between glass shards, coalescence of glassy material has not. Incipiently welded tuff is best developed where it comprises most of the section, reaching thicknesses of 20 m. In highly zoned sections, it occurs within the basal vitric part as thin, poorly defined layers,

Table 3 Summary of welding facies

Welding facies	Density g/cm³	Deformation of clasts		Adhesion of clasts	Typical color and luster
		Pumices	Shards		
Nonwelded	**<1.5** [1.43]	None	None	None to little	White to gray, dull
Incipiently welded	**1.50–1.65** [1.48, 1.57, 1.64]	None	None	Slight	Gray to pink, dull
Partially welded with pumice	**1.65–2.05** [1.63, 1.67, 1.74, 1.80, 1.83]	Slight	Slight	Moderate	Gray to dark gray, vitreous
Partially welded with fiamme	**2.05–2.30** [2.15, 2.20, 2.29] [2.07, 2.11, 2.12, 2.13]	Moderate	Slight	Strong	Dark gray to black, vitreous
Densely welded	**2.30–2.34** [2.34]	Moderate to strong	Strong	Complete	Black, vitreous

Bold values for density are the range for a particular facies. Values in brackets are measured values. Under partially welded with fiamme, the second set of values is for samples with pumice and fiamme. Luster refers to hand samples from the vitric zone

tens of centimeters thick. Unlike nonwelded tuff, incipiently welded tuff forms rugged cliffs with a distinctive erosion pattern. Meter-sized boulders break off exposed cliffs, but continued erosion apparently causes the rapid disintegration of boulders by the loosening of shards; cobbles are uncommon. Hand samples have a dull luster, but are vitric under a hand lens.

The zone of partial welding was divided into a zone with pumice and a zone with fiamme, reflecting increase in the degree of welding and development of eutaxitic structure (Table 3). The distinction is mappable and is important in intermediate to distal portions of the tuff (see regional facies). The partial welding zone spans the greatest change in density.

In the partially welded zone with pumice, pumice clasts are only slightly deformed; originally round bubbles are slightly ellipsoidal under the microscope.

There is some coalescence of glass in the shard matrix and hand samples are commonly vitreous. In some sections, as thick as 14 m, the main central part of the tuff consists of this welding facies. Weathering produces platy and angular forms with fragmentation ranging from boulders to pebbles. Although typically gray, in upper vitric sections partially welded tuff may be reddish owing to primary oxidation by upward percolating vapors during cooling of the tuff.

The welding facies 'partially welded with fiamme' is reached when most of the pumices are collapsed to fiamme, but the matrix still has some porosity (Fig. 9). Samples with transitional welding, with both pumice and fiamme, have intermediate densities (Table 3). Partially welded tuff with fiamme ranges from several meters thick in the central portion of sections greater than 60 km from the source to a thin (ca. 10–50 cm) zone

Fig. 9 'Partially welded with fiamme' welding degree. Most pumices have compacted to fiamme, indicating strong deformation, whereas the groundmass is middle gray indicating that the shards are only slightly deformed. The density of the specimen is 2.29 g/cm³. Consequently, the transition to the highest welding degree, densely welded, is only associated with a small increase in density (decrease in porosity), but is associated with the strong obliteration of grain boundaries. Coin is 2.4 cm in diameter

marking the transition to densely welded tuff in the base of highly zoned, proximal sections.

Dense welding results in tuff that is an obsidian-like black vitrophyre, lacking pore space. Fiamme and shards are thoroughly collapsed and eutaxitic texture is at times difficult to detect in hand samples. The vitric densely welded zone is thickest (ca. 4 m) where overlain by a pervasively devitrified zone and thins to 1 m where overlain by a spherulite or lithophysae zone.

Crystallization facies

Devitrification processes during cooling of the tuff led to the formation of four crystallization zones: the vapor phase zone; the pervasively devitrified zone; the spherulite zone; and the lithophysae zone. Transitions between crystallization zones are mainly gradational and vary from about 0.3 m to as thick as 2 m. In highly zoned tuff sections, the basal 2 m are typically vitric; spherulitic, pervasive and vapor phase crystallization generally occur successively higher in the section (Fig. 8). The lithophysae zone is superimposed on vitric, densely welded to pervasively devitrified tuff. The silica phase of the different crystallization types, reported in the following, are based on X-ray diffraction analysis of one representative sample from each zone.

The vapor phase zone is developed in upper incipiently welded and partially welded tuff. Proximal to the source area, it may have extended occasionally to the upper nonwelded facies, which is eroded. The term vapor phase zone is here not used *sensu stricto* because this zone comprises porous devitrified tuff with no or very limited mineral precipitation from a vapor phase ranging to porous devitrified tuff with obvious deposition of minerals in pore spaces (presumably from a vapor phase percolating through the cooling tuff). Therefore, crystallized tuff with pore space independent of the deposition of pore space minerals is referred to as vapor phase zone. This usage of the term vapor phase zone is similar to that defined by Smith (1980: 155): '... the crystalline porous zone is referred to as the *vapor-phase zone* ...'. This definition is more practical because whether vapor phase mineral deposition occurred or not is difficult to determine in the field; on the other hand, two subzones of this zone are distinguishable with a hand lens based on the crystal size, namely the cryptocrystalline and the microcrystalline vapor phase zones.

In the cryptocrystalline vapor phase zone, all glassy material crystallized, but the vitroclastic texture is perfectly preserved. Devitrification crystals are not recognizable in hand specimen. The very fine axiolitic structure of shards is revealed under the microscope (Fig. 10a); single crystals are less than 1 μm wide. The silica phase is cristobalite. In contrast, in the microcrystalline subzone, the axiolitic structures are coarser grained with crystals ca. 5–150 μm wide; the largest crystals occur along vesicle walls (Fig. 10b). The silica phase in the
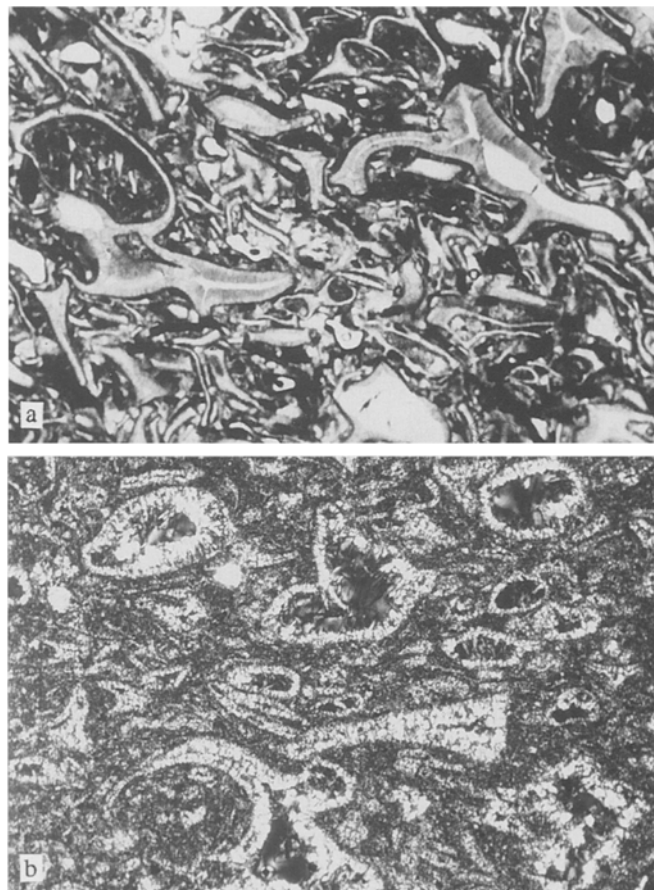

Fig. 10 a Cryptocrystalline vapor phase facies. Vitroclastic texture is retained despite 100% devitrification into very fine elongated crystals forming axiolitic structures, under plane light; white areas are vesicles. Silica phase is cristobalite. Horizontal field of view is ca. 3 mm. **b** Microcrystalline vapor phase facies. Same scale as above with crossed nicols, poorly developed vitroclastic texture seen only under microscope due to coarseness of more granular crystals. Note vesicles (black ovals) lined with largest crystals. Silica phase is mainly tridymite

microcrystalline subzone is tridymite, with a possible trace of cristobalite. The transition between the two vapor phase subzones is difficult to place. Where both occur, the microcrystalline overlies the cryptocrystalline subzone; the microcrystalline zone occurs to the exclusion of the cryptocrystalline subzone above pervasively devitrified tuff.

The pervasively devitrified zone is developed in tuffs that are densely welded or partially welded with fiamme and is distinguished by its stony appearance. There is good retention of flattened shard structure in thin section. It is denser than vapor phase tuff. The size of devitrification crystals is like that of the microcrystalline vapor phase subzone. The silica phase is cristobalite, with a possible trace of tridymite. The thickness of the pervasively devitrified zone ranges from ~15 m where it directly overlies black vitrophyre to 2–4 m where it overlies lithophysal tuff. Pervasively devitrified tuff has two styles of outcrop, a hackly jointed fa-

cies which underlies massive cliff facies (Figs. 2c and 8).

The spherulite zone develops almost exclusively in strongly welded vitric tuff at the contact between vitric and pervasively devitrified tuff. Spherulites range in size from about 1 mm to 2 cm. Only a few tuff sections were observed where spherulites formed without the formation of a lithophysae zone. The silica phase is cristobalite.

The lithophysae zone is the most complexly distributed crystallization zone. Unlike the other crystallization zones, lithophysae growth is overprinted on both vitric and devitrified tuff. Three stratigraphically consistent zones occur that vary in the type of rock overprinted by lithophysae: a lower zone, 1–2 m thick, of lithophysae in perlitic black densely welded vitric tuff that grades up to a middle zone, 2–3 m thick, of lithophysae in spherulitic tuff, which is overlain in abrupt contact by a zone as thick as 40 m of lithophysae in devitrified tuff (Fig. 15). Parts of the sequence were described by Beeson (1969) and Walker (1970, 1979).

Lithophysae are 1–3 cm and the silica phase is mainly tridymite, with a possible trace of cristobalite. The abundance increases upward from a few dispersed lithophysae in densely welded vitric tuff to a network of lithophysae in spherulitic tuff. Lithophysae in the lower two zones are mainly solid, with the minor development of hollow forms (Iddings 1885–1986: plates XII and XIV). The lithophysae in devitrified matrix are typically spherical (Fig. 11), but may range from solid to completely hollow with a crystallization rind lining the walls. Transitions include lithophysae with a hollow part or with a loose interior pellet.

Based on thin section and slab studies, lithophysae observed in devitrified matrix nucleated not in individual spots from where they grew outward, but several samples studied demonstrate that the first part of a lithophysa is always a crystallization rind surrounding some pervasively devitrified tuff (Fig. 11). This narrow rind grows mostly outward to form filled lithophysae, which may become partially and then completely hollow (Fig. 11). The loose interior pellet in hollow lithophysae represents the remaining core of pervasively devitrified tuff which was first surrounded by lithophysal crystallization. Commonly, there is a millimeter-scale, thin darker halo around lithophysae, indicating that the mafic constituents were expelled during lithophysae growth concentrating at the growth interface. Lithophysae formed in pervasively devitrified and spherulitic tuff are therefore mainly a recrystallization phenomenon forming tridymite at the expense of the cristobalite of previously crystallized tuff. The generation of hollow lithophysae solely through the release of volatiles as proposed by Ross and Smith (1980: 38) seems questionable in the light of the documented evolution from filled to hollow lithophysae. Therefore we distinguish between lithophysal cavities and gas cavities.

Previously, lithophysal and gas cavities were often used synonomously (e.g. Smith 1980: 156). Despite
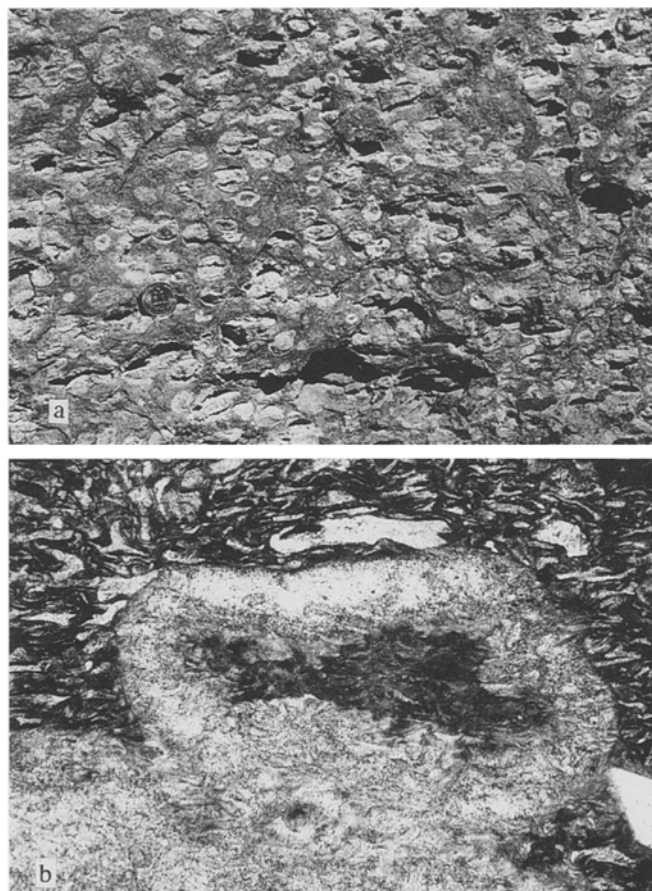

Fig. 11 a 'Lithophysae in devitrified tuff' facies. Lithophysae show continuum from lithophysal rind surrounding devitrified tuff to solid to completely hollow; matrix material is stony, pervasively devitrified tuff. Note larger gas cavity along bottom of picture. Coin for scale is 2.4 cm. **b** Close-up of beginning lithophysa in pervasively devitrified tuff. Lithophysa rind surrounds devitrified tuff. Note ghost shards between lithophysa rind and top of lower lithophysa. Horizontal field of view is ca. 6 mm

both being cavities, we suggest that their origin might be different. Gas cavities are solely the result of entrapment of gases; pore space minerals may be deposited from the vapor phase along their walls (e.g. Smith 1980). Lithophysal cavities (or hollow lithophysae), on the other hand, are an evolved stage of filled lithophysae.

In the non rheomorphic parts of the Rattlesnake Tuff, gas cavities are always completely hollow, round to ellipsoidal, often rugged in outline and are not associated with pore space minerals deposited from a vapor phase. Near the source, the largest gas cavities (10–40 cm) are common in the upper part of the lithophysae zone. In thick distal sections, gas cavities are small (ca. 4 cm) and elongate and occur in the absence of lithophysae or lithophysal cavities (see regional variations).

Rheomorphic tuff

The Rattlesnake Tuff has pronounced flowage features (e.g. Wolff and Wright 1981) at numerous places within 50 km of the vent (Figs. 12, 14 and 15). The dominant appearance of rheomorphic Rattlesnake Tuff is strongly lineated and folded devitrified tuff with locally abundant elongate openings parallel to foliation (Fig. 12). Whether the majority of these openings originated as gas cavities and were stretched later, or whether they formed by the separation of flow layers cannot be answered, although some have extremely high length to thickness ratios and are closely spaced along flow layers, suggesting the latter. In some thick, devitrified rheomorphic units these openings are lined with vapor phase minerals. Rheomorphic tuff may also be glassy, ranging from densely to nonwelded. Most dense, vitric rheomorphic tuff has the black color and vitric appearance of a densely welded vitrophyre plus typical elongated flow features. The most extraordinary rheomorphic tuff consists of a loose ashy matrix with flame-shaped lozenges that probably represent deformed pumices. There is almost no cohesion of the ash material. Only one occurrence on top of an entirely rheomorphic section could be documented.

Rheomorphic tuff is developed over normal non- to densely welded vitric tuff; it may be vitric or devitrified. Devitrified rheomorphic tuff may grade upward into a normal section, or into vitric rheomorphic 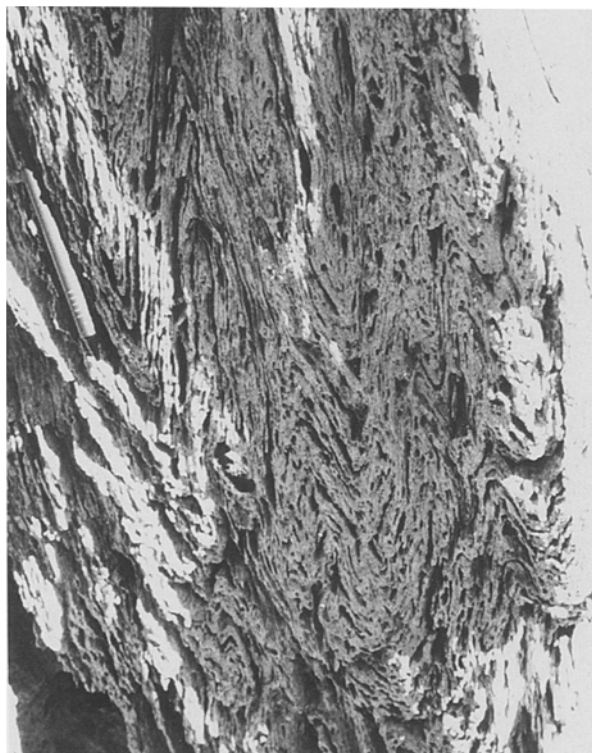tuff. Rheomorphic tuff sandwiched between normal tuff commonly has isoclinal to open folds and pumices are flattened, but commonly not strongly stretched.

Facies model

Welding and crystallization facies of the Rattlesnake Tuff vary locally and regionally. In general, the greatest diversity of facies is found closest to the source, where all facies occur, and decreases outward. Integration of the zonal variations of 85 individual sections produces an overall facies model that documents the vertical and horizontal variations in the welding and crystallization characteristics of the Rattlesnake Tuff (Fig. 15). The other 155 measured sections were not nearly as complete or diagnostic for vertical variations, but they were integrated into the model to help delineate regional variations.

Transitions between facies

The transition from one welding or crystallization facies to another can be smooth, gradational or abrupt. Transitional zones are typically more abrupt the more zones that are developed. Transitions between vitric to crystallized tuff can be extremely narrow, appearing often as a sharp (± 1 cm thick), horizontal interface in outcrop (Fig. 13). Sharp planar and subhorizontal contacts between glassy and devitrified zones are also reported from high-temperature ash-flows tuffs in Idaho (Bonnichsen and Citron 1982; Bonnichsen and Kauffmann 1987). Similar sharp boundaries between vitric and crystallized tuff have been interpreted as marking the contact of different flow units (Parker 1974; Toprak et al. 1994; Le Pennec et al. 1994); such an interpretation is not warranted if the evidence for different flow units is solely the lithological break from vitric to crystallized tuff.

Regional facies variations

To generalize the distribution of welding facies, approximate boundaries were drawn to indicate changes in the highest welding degree developed (Fig. 14). The degree of welding decreases with distance from the source, with the greatest change between 60 and 80 km from the source (Fig. 14), beyond which densely welded tuff (black vitrophyre) is rare. Instead, the highest degree of welding becomes partially welded tuff with fiamme and changes to partially welded tuff with pumice around 130 km.

Envelopes around the most distal outcrops of rheomorphic, lithophysal, vapor phase (without underlying devitrified tuff) and devitrified tuff are shown in Fig. 14. Beyond a distance of ca. 80 km lithophysae and lithophysal cavities are extremely rare and the occurrence of vapor phase tuff is minor and only above a

Fig. 12 Rheomorphic tuff. Small-scale normal folds in rheomorphic tuff. Pen is 14 cm in length

Fig. 13 Cryptocrystalline vapor phase zone (tan) overlying vitric tuff (gray). Sharp interface (at level of hammer) is only a lithological boundary separating lower vitric, partially welded tuff with pumice from upper cryptocrystalline vapor phase zone where holes indicate dissolution of pumice clasts. Picture is from the Fort Harney (FH) locality describid under Local facies variations. Similar vapor phase tuff is seen in Fig. 10a

lower pervasively devitrified zone. Closer to the vent, vapor phase zones also commonly occur directly above vitric tuff, reaching maximum thicknesses of ca. 10 m (Fig. 13). The occurrence of a vapor phase zone directly over vitric tuff proximal to the venting site has not been documented. Lithophysae are mainly developed in tuff sections reaching the highest degree of welding. There is no obvious correlation between thickness and degree of welding.

Rheomorphic tuff is restricted to an area within 40–60 km of the proposed vent and is largely limited to tuff sections >20 m, defining 10–20 km wide arcuate belts encircling the inferred vent (Fig. 3).

Local facies vatiations

At several localities, strong variations in welding and crystallization facies occur over a distance of a few

hundred meters with little or no change in thickness. Strong local topography and thickness variations can be excluded as a cause of these facies variations in most places. Four areas, at different distances from the inferred source, are described in the following from the closest to the most distal locality.

Silver Creek (SC) and Lunch Lake (LL) are located at the same distance from the inferred source (31 and 33 km, respectively) (Fig. 14). In both instances, the facies variations over a distance of 1–2 km exhibit the transition from a completely incipiently welded, vitric section to a highly zoned section with a lower non- to densely welded vitric zone overlain by a crystallized zone of dominantly lithophysal tuff (Fig. 15). Sections transitional between the endmembers include sections with lower partially welded tuff with pumice or with fiamme, both overlain by a vapor phase zone, and sections where non- to densely welded vitric tuff is overlain by pervasively devitrified tuff without lithophysae. In the Lunch Lake area, the described transitions take place along a flat-lying, ca. 15 m thick, continuously exposed Rattlesnake Tuff rim, which conformably overlies a basalt flow. There, within 200 m of continuous outcrop, the tuff varies from lower partially welded vitric tuff with fiamme overlain by cryptocrystalline vapor phase zone, to a section with densely welded vitric tuff overlain by pervasively devitrified tuff which is capped by a microcrystalline vapor phase zone and, finally, to a section with a several meter thick core of lithophysal tuff underlain by densely welded vitric and overlain by pervasively devitrified tuff. The described differences are not due to distance from the inferred vent because, in both areas, the completely incipiently welded section is closer to the vent than any of the more welded and more crystallized section.

At Fort Harney (FH), 63 km from the inferred source, Rattlesnake Tuff is 10–20 m thick (Fig. 14). Despite the greater distance, facies variation from an incipiently welded tuff to a section dominated by lithophysae occurs over 3 km (Fig. 15). A 100 m long outcrop of tuff displays how a vitric, partially welded section with pumice is split into lower and upper vitric tuff separated by a central wedge of cryptocrystalline vapor phase tuff (Fig. 13).

At Twin Buttes (TB), 83 km from the inferred source (Fig. 14), the lateral gradation in facies occurs over 50 m and the change is from a 15 m thick (base of tuff is exposed), entirely vitric section, composed mainly of partially welded tuff with pumice, to tuff with an upper 7 m thick pervasively devitrified zone and a vitric, partially welded zone with fiamme at the base (Fig. 15). A sharp interface, marking the vitric–crystallized transition, appears where the first crystallized tuff makes up the top of the section. From there, the interface runs towards thicker crystallized tuff downward at an angle of 25° relative to the horizontal tuff outcrop.
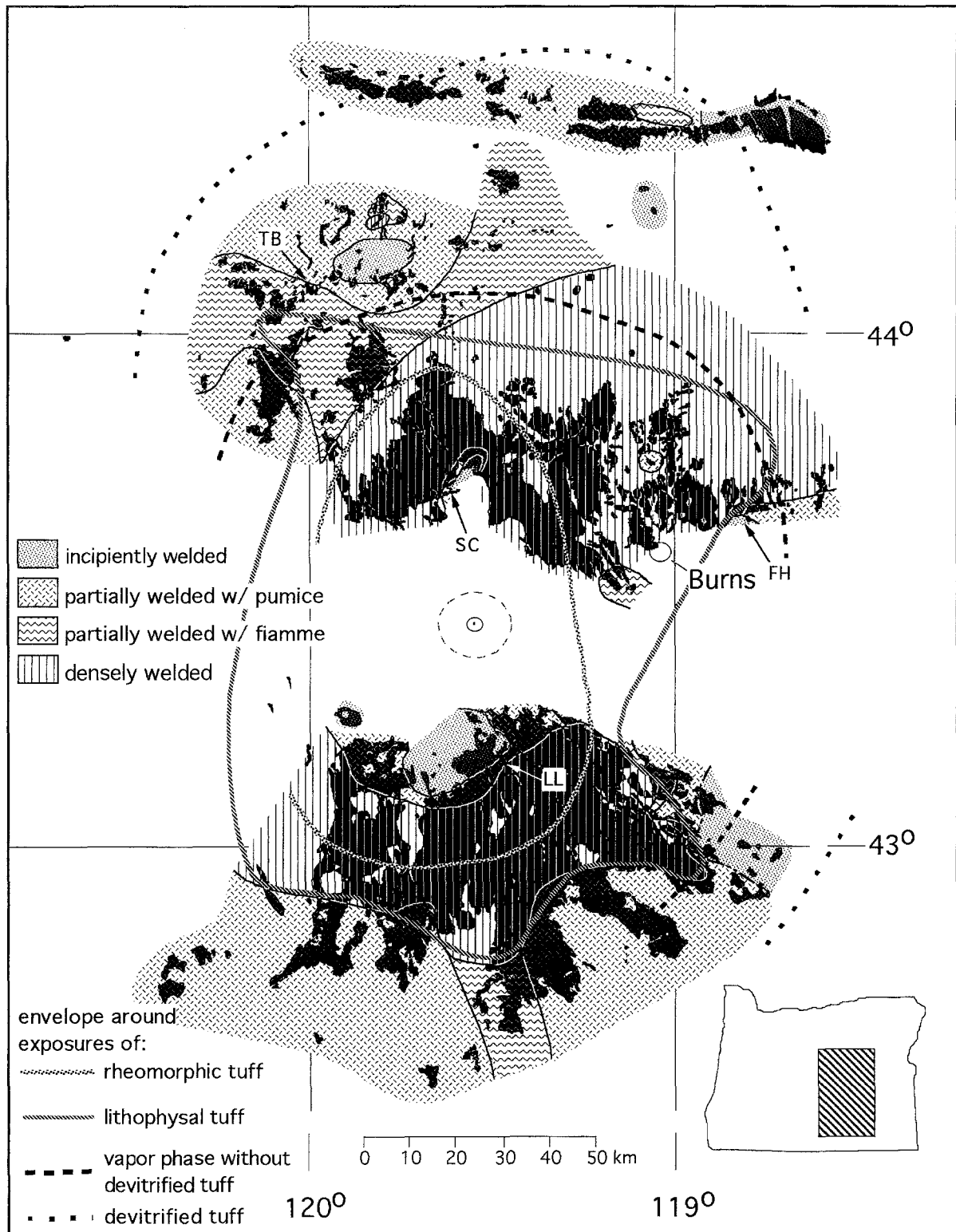
Fig. 14 Regional distribution of welding and crystallization facies. Distribution of welding is shown with respect to the highest welding degree observed at a given locality. The distribution of the highest welding facies is more interpretive in areas with thin outcrops (<5 m). Arrows with letters indicate areas mentioned under Local facies variations, viz.: LL, Lunch Lake; SC, Silver Creek; FH, Fort Harney; and TB, Twin Buttes. Rattlesnake Tuff outcrops are in black. Insert shows area of Fig. 14 relative to Oregon

Discussion of welding and crystallization facies

Comparison with existing facies models

Previously published facies models for ignimbrites are largely based on idealized hypothetical models established by Smith (1980). His models were constructed
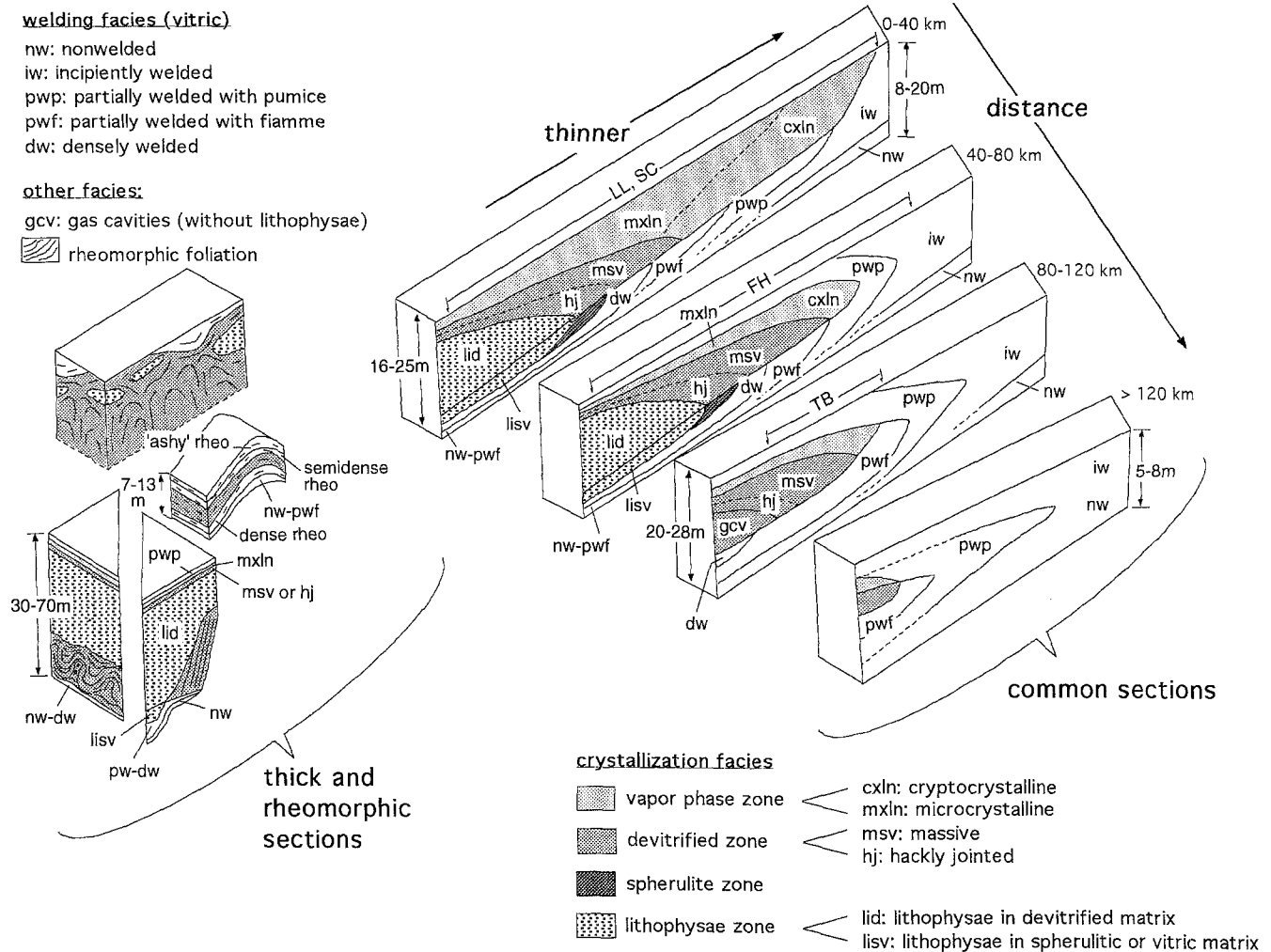
welding facies (vitric)

nw: nonwelded
iw: incipiently welded
pwp: partially welded with pumice
pwf: partially welded with fiamme
dw: densely welded

other facies:

gcv: gas cavities (without lithophysae)

rheomorphic foliation

crystallization facies

vapor phase zone — cxln: cryptocrystalline / mxln: microcrystalline

devitrified zone — msv: massive / hj: hackly jointed

spherulite zone

lithophysae zone — lid: lithophysae in devitrified matrix / lisv: lithophysae in spherulitic or vitric matrix

Fig. 15 Three-dimensional facies model. Areas without pattern are vitric. Pre-erosional upper nonwelded tuff omitted, except in one section displaying a characteristic rheomorphic section. Devitrified zone is synonymous with pervasively devitrified zone. Thicknesses indicate range of observed thicknesses of least eroded sections. The axis 'thinner' is the axis which describes local variations; regional variations are displayed by four intervals at increasing distance from the proposed source area. The distance intervals are based on the approximate distances where changes become noticeable (see regional variations). The principal variations in the Rattlesnake Tuff are represented by the 'common sections' and describe most of the tuff. Features of tuff outcrops that are unusually thick or outcrops displaying rheomorphic flow feature are illustrated with separate block diagrams as 'thick and rheomorphic sections'. The range in facies of the four localities (viz.: LL Lunch Lake; SC, Silver Creek; FH, Fort Harney; and TB Twin Buttes) described under Local facies variations are indicated by the arrows on top of the common section blocks

combining data from a large number of ash-flow deposits to show general differences in the distribution of welding and crystallization zones in endmember type ash-flow tuffs. Three endmember facies models include (1) a deposit which is thick, but too cold to develop strong welding and crystallization zones, (2) a thin, hot deposit which developed stronger welding zones, but without much crystallization and (3) a deposit which

was sufficiently thick, hot and gas-rich to develop dense welding and crystallization zones (Smith 1980: plate 20). All of the displayed variations within each model are attributed to a decrease in the temperature and thickness of the deposit with increased distance from the vent, even though some deposits indicate only very slight effects of cooling or thinning with distance (Smith 1980). In comparison, the zonal variations in the Rattlesnake Tuff (Fig. 15) document the complexity of a single ash-flow sheet in which facies vary abruptly over short distances and with no or little changes in thickness.

Timing

The relative time sequence of the welding and crystallization processes can be deduced from textural and field evidence. Welding is first. Any noticeable adhesion of glass shards during the last stages of flow, known as primary welding (Chapin and Lowell 1979) or as agglutination (e.g. Branney and Kokelaar 1992), is excluded because entirely incipiently welded sections also occur closest to the vent. Therefore, welding phenomena in the Rattlesnake Tuff are postdepositional.

Crystallization followed welding because it is superimposed on welding textures and some crystallization facies are associated with particular welding facies. The vapor phase zone occurs in tuff welded up to partially welded with pumice. At a higher welding degree, the pervasive devitrified zone develops instead. Individual spherulites are found only in densely welded vitric tuff. Where spherulite growth led to an interconnecting network of spherulites, the previous nature of the tuff is obliterated, but it appears that spherulite growth is restricted to densely welded, originally vitric tuff. Therefore, spherulite formation can be placed after welding and is likely to postdate the main formation of the pervasive devitrified zone (see later). Evidence from silicic lava flows also suggests that the formation of spherulites occurs in glassy material remaining after the central parts devitrified (Bonnichsen and Kauffmann 1987). The last crystallization process to occur is the development of lithophysae, which overprints vitric, spherulitic and pervasively devitrified tuff. That lithophysae in the Rattlesnake Tuff formed after and not during pervasive devitrification is based on the observation that the early stages of lithophysae are crystallization rinds that destroy the axiolitic devitrification of still recognizable shards (Fig. 11b). Lithophysae formation through recrystallization do not only occur in the pervasive devitrified zone, but also in the spherulite zone where spherulites are overprinted. The subtle and diffuse interface recognized in lithophysal tuff, separating spherulitic from pervasively devitrified tuff, probably represents the original sharp interface separating vitric from devitrified tuff, suggesting that pervasive devitrification is followed by later spherulite formation in some remaining glass, and crystallization of lithophysae is last.

Rheomorphism is predevitrification because crystallization facies overprint flow features (Fig. 15).

Causes of facies variations

A number of factors influence welding and crystallization, of which the most important are temperature, pressure, volatiles and composition (Ross and Smith 1980; Smith, 1960, 1980). Drastic local facies variations over <1–3 km of the Rattlesnake Tuff are crucial in evaluating the relative importance of these factors.

Differences in bulk magmatic composition are negligible because 99% or more of the tuff is high-silica rhyolite. There is no local concentration of dacitic pumice.

The influence of lithostatic load on the distribution of welding is thought to be minor because of the uniform thickness of the tuff along local facies variations. Differences in specific gravity indicate that densely welded tuff was never more than 1.7 times as thick as nonwelded tuff. Also, the missing nonwelded top was probably not markedly thicker over densely welded versus nonwelded sections, based on analogy with pre-

served basal nonwelded zones. A similar interpretation was reached for the Sifon ignimbrite, northern Chile, where the degree of welding is apparently unrelated to thickness (DeSilva 1989).

Volatiles can be divided into magmatic volatiles and inherited volatiles. Magmatic volatiles released from vesicles and from continued degassing of glass are likely to decrease with travel distance from the vent. However, it seems highly unlikely that the magmatic volatile composition or contents varied significantly on a local scale. On the other hand, volatiles derived from the substrate may change over short distances. The tuff may well have locally overrun marshy ground or shallow lakes and streams. Large potholes in the southeastern part of the outflow sheet have been interpreted as phreatic explosion pits (Johnson 1992). Evidence for water in the substrate is found in the John Day Basin (see under Depositional facies); in the Paulina Basin (Fig. 3), addition of water from the substrate is interpreted at a locality where the lower tuff of a 25 m section is abnormally altered and columnarly jointed above a nonwelded base. Walker (personal communication 1994) interpreted pumiceous Rattlesnake Tuff, which is completely altered to zeolites, as an example of deposition into shallow water. There is, however, no evidence that local water affected the localities with the strong facies variations described here.

Subtle changes in the temperature conditions of the tuff seem the most probable cause of the abrupt facies variations. The temperature of the tuff immediately after emplacement depends on the initial magmatic temperature, the heat lost during transport, the accumulation rate and the cooling rate. The accumulation and cooling rate depend on the emplacement mechanism. The high-energy character of the Rattlesnake Tuff and the lack of major topographic lows, where thick sections could accumulate, indicate a very similar emplacement mechanism locally. Therefore, we argue that regardless of the complex interplay of these factors, they are not likely to cause large differences in temperatures right after emplacement over the short distances characteristic of local facies changes. Although postemplacement thermal differences may have been small, they appear to have been enough to control local facies variations. Welding and crystallization could be controlled by a step-function behavior and occur when a tuff resides above a critical temperature for some minimum time. Thus fairly subtle differences in thickness (thermal insulation) could cause differential residence times above threshold temperatures for welding and crystallization. Differences in residence times could be affected by slightly different accumulation rates, by basal cooling by water, or by welding-induced reduction of permeability and thus reduction in convective cooling.

Conclusions

The Rattlesnake Tuff is a single cooling unit that was deposited from multiple high-energy ash flows. Pumice distribution and grading characteristics indicate that the transport medium consisted of highly expanded flows and the deposition medium consisted of much less expanded flows near the ground. The tuff erupted from an area near the center of today's outcrop distribution, based on a radial decrease in pumice clast size and general radial decrease of welding and crystallization. Vitric welding facies range from nonwelded to densely welded, with three intermediate welding degrees: incipiently welded; partially welded with pumice; and partially welded with fiamme. Crystallization facies are the early pervasively devitrified zone and the vapor phase zone, and the later spherulitic zone and lithophysae zone. All overprint welding. The pervasively devitrified zone is restricted to partially welded with fiamme to densely welded tuff. The vapor phase zone occurs in partially welded tuff with pumice or less welded tuff and is divided into two subzones, the cryptocrystalline and microcrystalline facies, distinguishable by the size of crystals. Spherulites occur in densely welded vitric tuff and lithophysae overprint vitric and all other crystallization facies, except possibly vapor phase tuff. Vitric to devitrified rheomorphic tuff occurs within 50 km of the source area and formed mainly syn- or postwelding and predevitrification.

Strong local variations, over <1–3 km, include the complete spectrum of regional variations, exhibited over tens to hundreds of kilometers. The drastic local variations suggest that facies variations result from subtle differences in emplacement, such as thickness or accumulation rate, which then result in sufficient residence above a critical temperature required for welding and crystallization.

References

Beeson MH (1969) A trace element study of silicic volcanic rocks of southeastern Oregon. PhD Thesis, Univ California, San Diego, 130 pp

Bloomfield K, Rubio GS, Wilson L (1977) Plinian eruptions of Nevado de Toluca Volcano, Mexico. Geol Rundsch 66:120–146

Bonnichsen B, Citron GP (1982) The Cougar Point Tuff, southwestern Idaho and vicinity. In: Bonnichsen B, Breckenridge RM (eds) Cenozoic Geology of Idaho. Idaho Bur Min Geol Bull 26:255–281

Bonnichsen B, Kauffmann DF (1987) Physical features of rhyolite lava flows in the Snake River Plain volcanic province, southwestern Idaho. Spec Pap Geol Soc Am 212:119–145

Booth B, Croasdale R, Walker GPL (1978) A quantitative study of five thousand years of volcanism on São Miguel, Azores. Phil Trans Roy Soc London A 288:271–319

Branney MJ, Kokelaar P (1992) A reappraisal of ignimbrite emplacement: progressive aggradation and changes from particulate to non-particulate flow during emplacement of high-grade ignimbrite. Bull Volcanol 54:504–520

Brown CE, Thayer TP (1966) Geologic map of the Canyon City quadrangle, northeastern Oregon. US Geol Surv Map I-447

Buesch DC (1992) Incorporation and redistribution of locally derived lithic fragments within a pyroclastic flow. Geol Soc Am Bull 104:1193–1207

Carlson RW, Hart WK (1987) Crustal genesis on the Oregon plateau. J Geophys Res 92:6191–6206

Cas RAF, Wright JV (1987) Volcanic Sucessions. Chapman and Hall, London, 528 pp

Chapin CE, Lowell GR (1979) Primary and secondary flow structures in ash-flow tuffs of the Gribbles Run paleovalley, central Colorado. Spec Pap Geol Soc Am 180:137–154

Davenport RE (1971) Geology of the Rattlesnake and older ignimbrites in the Paulina basin and adjacent area, central Oregon. PhD Thesis, Oregon State Univ, Corvallis, 132 pp

DeSilva SL (1989) Geochronology and stratigraphy of the ignimbrites from the 21°30′S to 23°30′S portion of the central Andes of northern Chile. J Volcanol Geotherm Res 37:93–131

Draper DS (1991) Late Cenozoic bimodal magmatism in the northern Basin and Range Province of southeastern Oregon. J Volcanol Geotherm Res 47:299–328

Ekren EB, McIntyre DH, Bennett EH (1984) High-temperature, large-volume, lavalike ash-flow tuffs without calderas in southwestern Idaho. US Geol Surv Prof Pap 1272:1–73

Enlows HE (1976) Petrography of the Rattlesnake Formation at the type area central Oregon. Oregon Dept Geol Min Ind Short Pap 25:1–34

Fisher RV (1966) Geology of a Miocene ignimbrite layer, John Day Formation, eastern Oregon. Univ Calif Publ Sci Geol 47:1–58

Fisher RV, Orsi G, Ort M, Heiken G (1993) Mobility of large-volume pyroclastic flow – emplacement of the Campanian ignimbrite, Italy. J Volcanol Geotherm Res 56:205–220

Greene RC (1973) Petrology of the welded Tuff of Devine Canyon, southeastern Oregon. US Geol Surv Prof Pap 797:1–26

Greene RC, Walker GW, Corcoran RE (1972) Geologic map of the Burns quadrangle, Oregon. US Geol Surv Map I-680

Hart WK, Aronson JL, Mertzman SA (1984) Areal distribution and age of low-K, high-alumina olivine tholeiite magmatism in the northwestern Great Basin. Geol Soc Am Bull 95:186–195

Iddings JP (1885–1886) Obsidian Cliff, Yellowstone National Park. US Geol Surv 7th Annu Rep 249–295

Johnson GD (1960) Geology of the northwest quarter Alvord Lake Three quadrangle, Oregon. Master's Thesis, Oregon State Univ, Corvallis, 75 pp

Johnson JA (1992) Geology of the Krumbo reservoir quadrangle southeastern Oregon. BSc Thesis, Oregon State Univ, Corvallis, 55 pp

Kuno H, Ishikawa T, Katsui Y, Yagi K, Yamasaki M, Taneda S (1964) Sorting of pumice and lithic fragments as a key to eruptive and emplacement mechanism. Jpn J Geol Geogr 35:223–238

Lawrence RD (1976) Strike-slip faulting terminates the Basin and Range province in Oregon. Geol Soc Am Bull 87:846–850

Le Pennec J-L, Bourdier J-L, Froger J-L, Temel A, Camus G, Gourgaud A (1994) Neogene ignimbrites of the Nevsehir plateau (central Turkey): stratigraphy, distribution and source constraints. J Volcanol Geotherm Res 63:59–87

Lirer L, Pescatore T, Booth B, Walker GPL (1973) Two Plinian pumice-fall deposits from Somma-Vesuvius, Italy. Geol Soc Am Bull 84:759–772

MacLeod NS, Walker GW, McKee EH (1976) Geothermal significance of eastward increase in age of upper Cenozoic rhyolitic domes in southeastern Oregon. Second United Symp Development and Use of Geothermal Resources, Proc 1:465–474

Mansfield GR, Ross CS (1935) Welded tuffs in southeastern Idaho. Am Geophys Union Trans 16th Annu Mtg, Natl Res Coun 308–321

Parker DJ (1974) Petrology of selected volcanic rocks of the Harney Basin, Oregon. PhD Thesis, Oregon State Univ, Corvallis, 153 pp

Riehle JR (1973) Calculated compaction profiles of rhyolitic ash-flow tuffs. Geol Soc Am Bull 84:2193–2216

Ross CS, Smith RL (1980) Ash-flow tuffs: their origin, geologic relations and identification. Rep US Geol Surv Prof Pap 366 (1960) New Mex Geol Soc Spec Publ 9:159 pp

Samson SD, Alexander EC Jr (1987) Calibration of the interlaboratory ^{40}Ar–^{39}Ar dating standard, MMhb-1. Chem Geol Isotope Geosci 66:27–34

Smith G, Taylor E, Thormahlen D, Enlows H (1984) Three newly recognized occurrences of Rattlesnake ignimbrite in central Oregon. Proc Oreg Acad Sci XX:55

Smith RL (1960) Ash flows. Geol Soc Am Bull 71:795–842

Smith RL (1979) Ash-flow magmatism. Spec Pap Geol Soc Am 180:5–27

Smith RL (1980) Zones and zonal variations in welded ash-flows. Rep US Geol Surv Prof Pap 354-F (1960) New Mex Geol Soc Spec Publ 9:1–159

Sparks RSJ (1975) Stratigraphy and geology of the ignimbrites of Vulsini volcano, central Italy. Geol Rundsch 64:497–523

Spera FJ, Crisp JA (1981) Eruption volume, periodicity, and caldera area: relationships and inferences on development of compositional zonation in silicic magma chambers. J Volcanol Geotherm Res 11:169–187

Stearns HT, Isotoff A (1956) Stratigraphic sequence in the Eagle Rock volcanic area near American Falls, Idaho. Geol Soc Am Bull 67:19–34

Streck MJ (1994) Volcanology and petrology of the Rattlesnake Ash-Flow Tuff. PhD Thesis, Oregon State Univ, Corvallis, 185 pp

Suzuki-Kamata K, Kamata H (1990) The proximal facies of the Tosu pyroclastic-flow deposit erupted from Aso caldera, Japan. Bull Volvanol 52:325–333

Swanson DA (1969) Reconnaissance geologic map of the east half of the Bend quadrangle, Crook, Wheeler, Jefferson, Wesco, and Deschutes counties, Oregon. US Geol Surv Map I-568

Taylor JR (1982) An Introduction to Error Analysis. University Science Books, Mill Valley, California

Thayer TP (1952) The tuff member of the Rattlesnake Formation of eastern Oregon – an ignimbrite. Trans Am Geophys Union 33:327

Toprak V, Keller J, Schumacher R (1994) Volcano-tectonic features of the Cappadocian volcanic province. Excursion Guide, IAVCEI, Ankara, 58 pp

Wallace RE, Calkins JA (1956) Reconnaissance map of the Izee and Logell quadrangles, Oregon. US Geol Surv Map MF-82

Walker GPL (1980) The Taupo Pumice: product of the most powerful known (ultraplinian) eruption. J Volcanol Geotherm Res 8:69–94

Walker GPL (1983) Ignimbrite types and ignimbrite problems. J Volcanol Geotherm Res 17:65–88

Walker GW (1963) Reconnaissance geologic map of the eastern half of the Klamath Falls quadrangle, Lake and Klamath counties. US Geol Surv Map MF-260

Walker GW (1969) Possible fissure vent for a Pliocene ash-flow tuff, Buzzard Creek area, Harney county, Oregon. US Geol Surv Prof Pap 650-C:8–17

Walker GW (1970) Cenozoic ash-flow tuffs of Oregon. Oreg Dept Geol Min Ind 32:97–115

Walker GW (1974) Some implications of late Cenozoic volcanism to geothermal potential in the High Lava Plains of south-central Oregon. Oreg Dept Geol Min Ind 36:109–123

Walker GW (1979) Revisions to the Cenozoic stratigraphy of Harney basin, southeastern Oregon. US Geol Surv Bull 1475:1–35

Walker GW, Repenning CA (1965) Reconnaissance geologic map of the Adel quadrangle, Lake, Harney, and Malheur counties. US Geol Surv Map I-446

Walker GW, Peterson NV, Greene, RC (1967) Reconnaissance geologic map of the east half of the Crescent quadrangle, Lake, Deschutes, and Crook counties, Oregon. US Geol Surv Map I-493

Wilcox RE, Fisher RV (1966) Geologie map of the Monument quadrangle, Grant county, Oregon. US Geol Surv Map GQ-541

Wolff JA, Wright JV (1981) Rheomorphism of welded tuffs. J Volcanol Geotherm Res 10:13–34

Wright JV, Walker GPL (1977) The ignimbrite source problem: significance of a co-ignimbrite lag-fall deposit. Geology 5:729–732

Yokoyama S (1974) Flow and emplacement mechanism of the Ito pyroclastic flow from Aira caldera, Japan. Tokyo Kyoiku Daigaku Sci Rep Sec C 12:17–62